ELSEVIER

Cell Calcium 40 (2006) 413–422

cell calcium

www.elsevier.com/locate/ceca

Imaging single-channel calcium microdomains

Angelo Demuro, Ian Parker *

Department of Neurobiology and Behavior, University of California, Irvine, CA 92697-4550, United States

Received 1 August 2006; accepted 23 August 2006
Available online 25 October 2006

Abstract

The Ca^{2+} microdomains generated around the mouth of open ion channels represent the basic building blocks from which cytosolic Ca^{2+} signals are constructed. Recent improvements in optical imaging techniques now allow these microdomains to be visualized as single channel calcium fluorescence transients (SCCaFTs), providing information about channel properties that was previously accessible only by electrophysiological patch-clamp recordings. We review recent advances in single channel Ca^{2+} imaging methodologies, with emphasis on total internal reflection fluorescence microscopy (TIRFM) as the technique of choice for recording SCCaFTs from voltage- and ligand-gated plasmalemmal ion channels. This technique of 'optical patch-clamp recording' is massively parallel, permitting simultaneous imaging of hundreds of channels; provides millisecond resolution of gating kinetics together with sub-micron spatial resolution of channel locations; and is applicable to diverse families of membrane channels that display partial permeability to Ca^{2+} ions.

Keywords: *Xenopus* oocyte; Optical single-channel recording; N-type Ca^{2+} channel; nAChRs; TIRFM; Confocal microscopy; Calcium microdomains

1. Introduction

Calcium is unique among other intracellular second messengers in regard to the rapidity and tight spatial localization of cytosolic Ca^{2+} signals. This is possible because active transport systems maintain enormous (ca. 10,000-fold) Ca^{2+} concentration gradients between the cytosol and reservoirs in the extracellular fluid and endoplasmic reticulum, so that openings of Ca^{2+}-permeable membrane channels permit passive flux to generate large and rapid elevations of local cytosolic [Ca^{2+}]. For example, a single-channel Ca^{2+} current of 0.5 pA during an opening of 10 ms duration corresponds to a flux of $\sim 10^4$ Ca^{2+} ions; a transport rate that greatly exceeds that of enzymatic synthesis of other messenger molecules, and thereby endows Ca^{2+} signals with exquisite temporal specificity. Moreover, the presence of immobile cytosolic Ca^{2+} buffers greatly inhibits the diffusional spread of Ca^{2+} ions at distances of more than a few hundred nm, resulting in sharply defined microdomains of Ca^{2+} around local sites of Ca^{2+} influx or release. These spatially- and temporally-defined microdomains serve to regulate numerous diverse cell processes [1–9].

Following the introduction of highly-sensitive fluorescent Ca^{2+} indicator dyes [10] it became possible to directly image Ca^{2+} microdomains within cells. Initial experiments revealed 'elementary' Ca^{2+} signals [11] such as puffs [12] and sparks [13] that are believed to be generated by the concerted openings of several, tightly clustered Ca^{2+} release channels. Soon after, yet smaller 'fundamental' events (blips and quarks) were observed, and were interpreted to arise from the openings of single channels [12,14,15]. However, the first conclusive demonstrations of single-channel Ca^{2+} signals were provided by Zou et al. and Wang et al. [16,17] who combined optical and electrophysiological techniques to obtain simultaneous recording of current flow through a single open ion channel together with imaging of *s*ingle-*c*hannel *C*a^{2+} *f*luorescent *t*ransients (SCCaFTs).

Subsequent experiments have improved considerably on the fidelity with which SCCaFTs can be imaged, and contin-

Abbreviations: TIRFM, total internal reflection microscopy; SCCaFT, single channel calcium fluorescence transient; ACh, acetylcholine

* Corresponding author. Tel.: +1 949 824 7332; fax: +1 949 824 2447.
E-mail address: iparker@uci.edu (I. Parker).

0143-4160/$ – see front matter © 2006 Elsevier Ltd. All rights reserved.
doi:10.1016/j.ceca.2006.08.006

uing developments are driven by two principal motivations. One is to define better the cytosolic microdomains that constitute the basic 'building blocks' of cellular Ca^{2+} signaling. What are their amplitudes? What is their spatial spread? Where are the Ca^{2+} channels located and are they motile? A second aspect is that SCCaFTs can provide information about channel gating and Ca^{2+}-permeation properties analogous to that obtained by electrophysiological patch-clamp recordings, but with the great advantage that imaging is massively parallel, capable of recording from hundreds of channels at once.

Key requirements for both these purposes are to optimize the spatial and temporal resolution of the imaging system. Indeed, these aspects are tightly intertwined. Ca^{2+} concentrations in the close vicinity of a channel mouth are large and rapidly track channel openings and closings, but Ca^{2+} transients become increasingly smaller and slowed by diffusion at increasing distances. Imaging techniques with improved resolution in both lateral (x–y) and axial (z) dimensions are thus expected to provide not only a better spatial localization, but also an enhanced temporal resolution by virtue of monitoring Ca^{2+}-dependent fluorescence from tinier sampling volumes immediately adjacent to the channel. Several techniques have been used to image SCCaFTs, including wide-field microscopy [17,18], confocal linescan microscopy [16,19], and total internal reflection fluorescence microscopy (TIRFM) [20–23]; see [24–27] for reviews. Each methodology has particular advantages related to specific applications, but we concentrate on recent developments in TIRF microscopy as this is currently the most advantageous technique for imaging plasmalemmal Ca^{2+} microdomains, permitting fast, two-dimensional imaging of fluorescence signals within an exceedingly thin (ca. 100 nm) optical section adjacent to the cell membrane [24].

2. Spatial distribution of free Ca^{2+} and Ca^{2+}-bound indicator around the channel mouth

Before reviewing experimental approaches to image SCCaFTs it is helpful to consider some theoretical aspects of single-channel Ca^{2+} microdomains, as numerical models provide our only insight into the underlying processes at time and distance scales below the limits of optical resolution. A number of studies have modeled Ca^{2+} diffusion in the cytosol during channel opening with the aim of predicting the rapid time course of Ca^{2+}-dependent processes such as transmitter release and Ca^{2+}-induced receptor trafficking [28,29]. More recently, theoretical approaches have been extended to consider the relation between the free Ca^{2+} microdomain around a channel and the resulting fluorescence signal, so as to aid interpretation of the fluorescence images and guide improvement of the imaging techniques [30,31].

On the basis of modeling studies by Shuai and Parker [30], we illustrate schematically in Fig. 1 how Ca^{2+} flux through a single channel leads to the generation of experimentally-observed SCCaFTs. The predicted distribution of free $[Ca^{2+}]$ is shown in Fig. 1A at a time 10 ms following the opening of a plasma membrane channel passing a Ca^{2+} current of 0.1 pA. The peak $[Ca^{2+}]$ exceeds 100 μM near the channel mouth, but falls abruptly to <1 μM at a distance of ∼100 nm. In comparison, the distribution of Ca^{2+}-bound indicator dye (Fig. 1B) is much broader (full-width at half-maximal amplitude, FWHM = 270 nm), owing to the kinetics of Ca^{2+} binding and the faster effective diffusion coefficient of the indicator as compared to that of buffered Ca^{2+} diffusion. To reflect experimental conditions, we then introduce optical blurring by the microscope (Fig. 1C), in this case considering the point-spread function of a TIRF microscope (300 nm lateral resolution and 100 nm axial; [30]), resulting in a SCCaFT width (FWHM) of ∼500 nm. This predicted width of the fluorescence signal matches well with the spatial profiles of SCCaFTs obtained experimentally during opening of muscle nicotinic receptors (green curve, Fig. 1D: FWHM ∼600 nm: [21]. Thus, fluorescence images of SCCaFTs are appreciably broader than the underlying distribution of free $[Ca^{2+}]$ (Fig. 1D and E), a blurring that involves roughly equal contributions from the spread of Ca^{2+}-bound indicator dye and the diffraction-limited resolution of optical microscopy.

The temporal resolution with which SCCaFTs can be recorded depends also on spatial constraints, and simulations [30] show that the kinetics of SCCaFTs recorded from localized cytosolic volumes improve progressively with decreasing size of the sampling volume. However, this involves a compromise, because smaller volumes encompass less indicator dye and statistical fluctuations in the number of Ca^{2+}-bound indicator molecules ('molecular shot noise') degrade the signal-to-noise ratio. Volumes around 0.1 fl (10^{-16} l) appear to offer a good compromise, and match well to the volumes of the focal spot achieved with confocal or TIRF microscopy. Under minimally-perturbing conditions the model simulations predict that SCCaFTs should track channel openings and closings with a temporal resolution approaching 1 ms, and yet faster resolution may be achieved by use of high (mM) cytosolic indicator concentrations and by introduction of slow, mobile Ca^{2+} buffers such as EGTA [30].

3. Single Ca^{2+} channel imaging methodologies

Fig. 2 shows some of the imaging techniques that have been applied to record single-channel Ca^{2+} transients, and illustrates progressive improvements in resolution achieved over the past few years.

By employing high-speed, wide-field fluorescence microscopy Zou et al. [17] were able to record localized fluorescence transients associated with the opening of sparsely-distributed stretch-activated cation channels in smooth muscle cells (Fig. 2A). This technique provides little or no axial 'sectioning' of the fluorescence image, so that signals

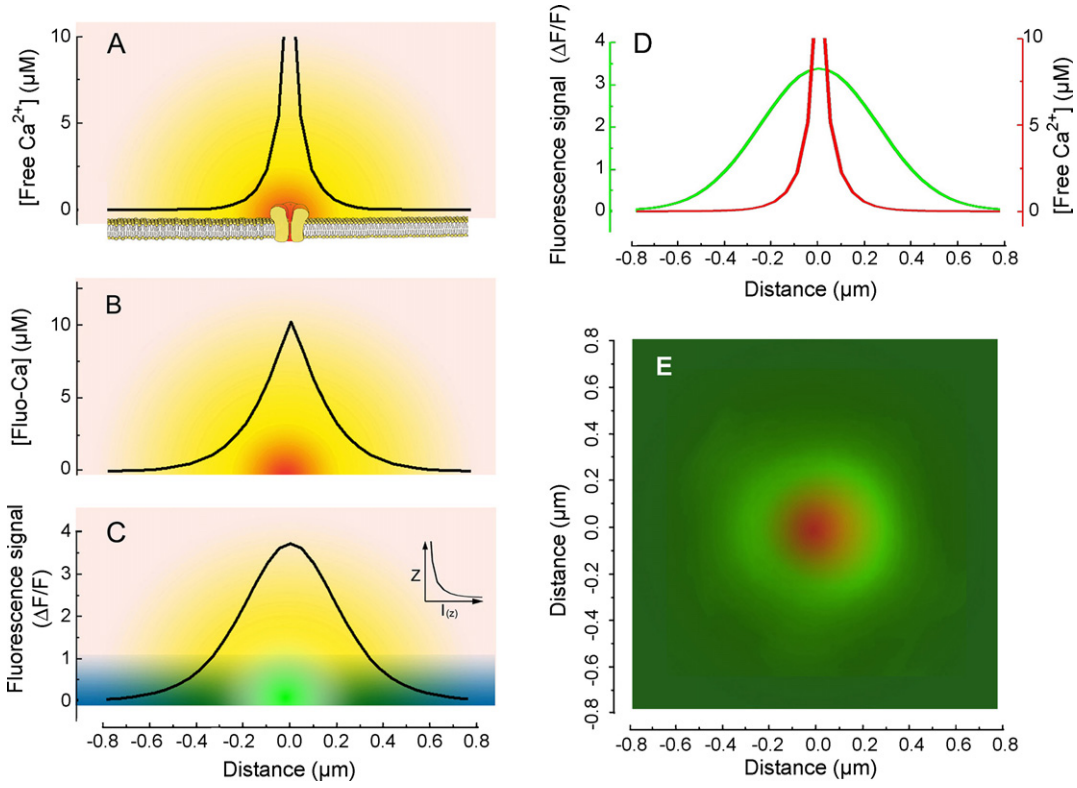

Fig. 1. Imaging single-channel Ca^{2+} microdomains: relationships between the spatial distribution of free [Ca^{2+}] and the resulting fluorescence image. (A) Schematic depicting the concentration profile of free [Ca^{2+}] as a function of distance from the mouth of a Ca^{2+} channel carrying a current of 0.1 pA for 10 ms. (B) Corresponding distribution of concentration of Ca^{2+}-bound indicator dye (Fluo-4). The total indicator concentration is 25 μM. (C) Spatial profile of fluorescence (green) that would be imaged from the Ca^{2+}-bound indicator by total-internal reflection microscopy. The blue gradient and the inset graph depict the depth penetration of the evanescent wave employed to excite fluorescence. (D) Comparison of the simulated spatial distribution of free Ca^{2+} (red curve) and the experimentally-observed fluorescence signal (SCCaFT: green curve) resulting from opening of a nicotinic ACh channel. The green curve is a Gaussian fit (FWHM = 600 nm) to an average of 6 SCCaFTs. (E) Image overlay shows the predicted two-dimensional distribution of free Ca^{2+} (red) in the microdomain around a single channel, together with an experimentally-observed SCCaFT (green) imaged by TIRFM microscopy. Simulation data in (A–C) are adapted from Ref. [30]; the experimental SCCaFTs in (D and E) were obtained by imaging adult muscle nAChRs (A.D. & I.P.; unpublished data). (For interpretation of the references to color in this figure legend, the reader is referred to the web version of the article.)

are recorded from large cytosolic volumes and are therefore relatively slow—primarily reflecting Ca^{2+} accumulation in the cytosol rather than instantaneous Ca^{2+} flux. Nevertheless, measurements of rate-of-rise of fluorescence at the source track channel gating more faithfully, and wide-field imaging directly provides a measure of 'signal mass' [32] that is directly proportional to the cumulative Ca^{2+} flux during a channel opening [33]. Significant improvements in spatial and temporal resolution were subsequently obtained by using 'optical sectioning' techniques, including confocal and TIRF microscopy to image fluorescence signals from sub-femtoliter volumes near the channel mouth. Fig. 2B shows simultaneous recordings of Ca^{2+} fluorescence signal and unitary Ca^{2+} currents associated with depolarization-induced opening of L-type Ca^{2+} channels in rat myocytes [16]. Fluorescence was imaged by confocal linescan microscopy, and single channel signals (here called 'sparklets') were enhanced by increasing the Ca^{2+} concentration in the bathing to 20 mM, and by prolonging the channel open time with the L-type channel agonist FPL64176. Confocal linescan imaging was similarly employed to record SCCaFTs generated by openings of N-type Ca^{2+} channel transiently expressed in *Xenopus* oocytes (Fig. 2C) [19,24]. Using scan rates of 2 ms per line events with durations <10 ms were resolved, with rising and falling time of about 4 ms (Fig. 2C; left inset), although the decay of the fluorescence slowed to ~10 ms at the end of longer events (Fig. 2C; inset at right).

Although linescan confocal microscopy offers a good combination of small sampling volume (point-spread function <0.1 fl) and fast instrumental time resolution (~1 ms per line), it samples from only one spatial dimension. Disadvantages are thus that only few channels may lie close to the scan line, and recordings may be distorted by off-focus signals arising from channels some distance from the scan line. A major improvement in optical single-channel imaging has been achieved by using total internal reflection microscopy coupled with ultra-fast, high-sensitivity cameras for two-dimensional fluorescence imaging of plasmalemmal SCCaFTs [20,21,23]. For example, Fig. 3D illustrates SCCaFTs generated by Ca^{2+} flux through nicotinic acetylcholine receptors (nAChRs) expressed in *Xenopus* oocytes [21]. Channel openings were evoked by adding 30 nM ACh to

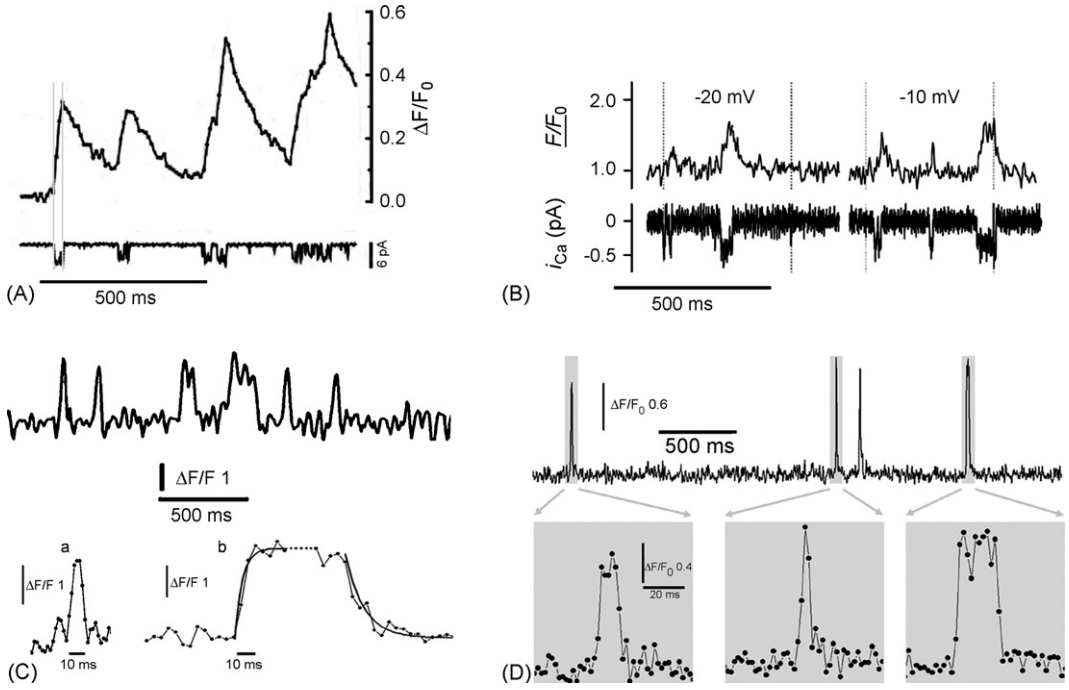

Fig. 2. Time-resolved single-channel Ca^{2+} fluorescence transients obtained using different imaging techniques. (A) SCCaFTs imaged by wide-field fluorescence microscopy during openings of a stretch-activated cation channel. Fluorescence images were acquired at 15 ms frame intervals (upper trace), in conjunction with single-channel current measurements obtained by whole-cell patch-clamp. Data are reproduced with permission from Ref. [17]. (B) Confocal linescan record (1.4 ms per line) of fluorescence transients ('sparklets': upper trace) generated by the opening of an L-type Ca^{2+} channel in cardiac muscle and simultaneous recording of the unitary Ca^{2+} current (lower trace) during 400 ms depolarization pulses from −50 mV to the indicated voltages. The patch pipette contained 20 mM Ca^{2+} and 10 μM FLP to, respectively, enhance Ca^{2+} flux and prolong channel openings. Data are reproduced with permission from Ref. [16]. (C) Confocal linescan recordings (2 ms per line) of SCCaFTs from N-type Ca^{2+} channels expressed in *Xenopus* oocytes. Upper trace shows several SCCaFTs evoked during depolarization to −10 mV in the presence of 8 mM extracellular [Ca^{2+}]: lower traces show a single, brief sparklet (a) and averages of nine longer sparklets (b) formed after aligning their rising phases (left) and falling phases (right). Exponential curves fitted to the rising and falling phases have respective time constants of 4 and 10 ms. Reproduced with permission from Ref. [19]. (D) Imaging of SCCaFTs through muscle nAChR expressed in *Xenopus* oocytes by TIRF microscopy using a c.c.d. camera operating at 500 frames s^{-1}. Upper trace shows several SCCaFTs monitored from a (0.7 μm × 0.7 μm) region around a single nAChR in the presence of 300 nM ACh and 8 mM [Ca^{2+}]; lower traces show expanded views of selected events as indicated by the grey boxes. Reproduced with permission from Ref. [21].

the bathing solution and the membrane potential was stepped to – 150 mV to increase the electrochemical driving force for Ca^{2+} influx. The inset traces (Fig. 3D) show expanded version of selected SCCaFTs in the upper trace, revealing a temporal resolution of ∼2 ms.

4. TIRF microscopy for 'optical patch-clamp' recording

Our work focuses on the use of *Xenopus* oocytes as a model cell system to image single-channel Ca^{2+} flux through expressed voltage- and ligand-gated Ca^{2+}-permeable channels [19–21,24,30,34]. Important advantages of this preparation include the ready ability of the oocyte to express a large variety of channel types, the relative scarcity of endogenous ion channels in the plasma membrane, and the enormous size of the oocyte that results in a low channel density even for very high overall levels of expression. In conjunction, we find that TIRF microscopy is currently the most favorable technique for imaging the activity of plasma membrane channels, because the restriction in fluorescence excitation to a very thin (ca. 100 nm) evanescent wave resulting from total internal reflection at the refractive index boundary between the microscope cover glass and the aqueous specimen minimizes the sampling volume [35]. Moreover, a two-dimensional (x–y) image of this thin optical section can be recorded by a camera, rather than requiring the raster-scanning of a confocal laser spot where mechanical constraints limit the maximal imaging speed. The basic principle of TIRFM has been reviewed recently [24,35], and here we emphasize practical details regarding our application of this method for imaging single-channel Ca^{2+} microdomains [20,21].

We utilize defolliculated stage VI oocytes from *Xenopus laevis* because these largely lack the abundant microvilli seen in the oocyte membrane at earlier developmental stages, thereby minimizing damage during removal of the surrounding vitelline envelope and facilitating close apposition of the oocyte membrane to the coverglass for TIRFM imaging. About 24 h after injecting mRNA or cDNA encoding for the desired channels, oocytes are mechanically stripped from the vitelline membrane and positioned with the animal pole

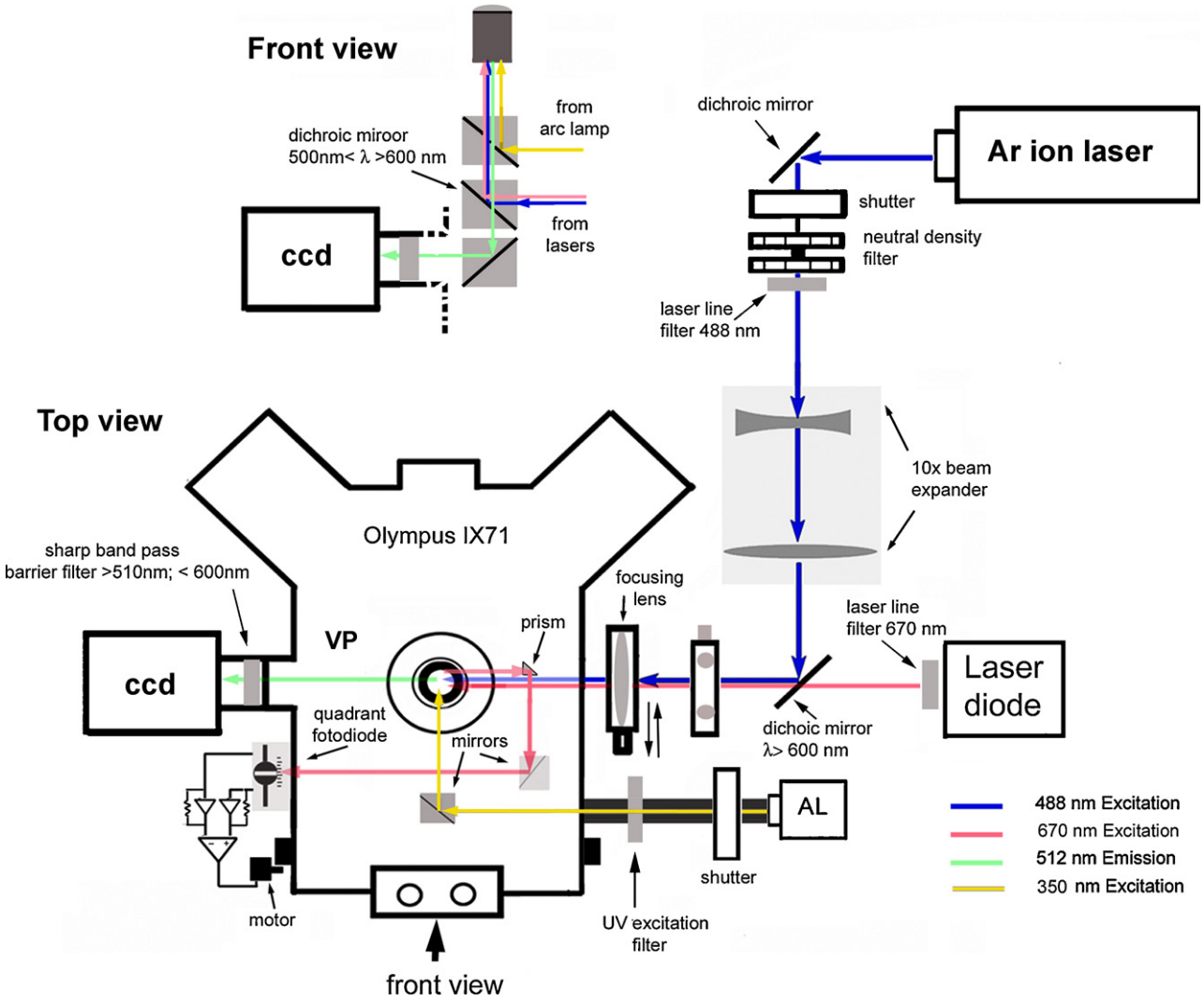

Fig. 3. Schematic view of TIRF microscope system used for time-resolved single-channel imaging. This is based around an Olympus IX 71 inverted microscope equipped with an Olympus 60× TIRFM objective (NA = 1.45). Excitation light (488 nm) from a 50 mW argon ion laser is attenuated by a neutral density filter, expanded by a 10× beam expander and focused by a lens via a dichroic mirror to a spot at the back focal plane of the objective lens. Translation of the focusing lens allows the beam to be introduced either at the extreme edge of the objective aperture (for TIR excitation), or more centrally (for 'wide field') excitation. An adjustable rectangular knife-blade aperture located at the conjugate image plane restricts the excitation to the field imaged by the camera. Laser light is directed into the objective by the primary dichroic mirror (λ = 500 nm) in the epifluorescence turret (front view). The emitted fluorescence is collected through the objective lens, and passes through the primary dichroic and a barrier filter (>510 nm) to focus on an ultrafast back-illuminated, electron-multiplied c.c.d. camera (Cascade 128+, Roper Scientific). To correct for focus drift while imaging an autofocus system utilizes a red laser diode as a reference beam. After undergoing TIR at the coverglass/water interface, the reflected laser beam emerging from the objective is directed onto a quadrant photodiode, establishing a negative feedback for fine control of the focus motor. A third light path allows delivery of UV light flashes for rapid photolysis of caged agonists such as caged carbamycholine.

facing a clean coverglass forming the bottom of the recording chamber. A conventional two-electrode voltage clamp allows the membrane potential to be clamped to strongly hyperpolarized potentials to increase the electrochemical driving force for Ca^{2+} entry through ligand-gated channels, or to be depolarized to activate voltage-gated channels.

The TIRFM imaging system (Fig. 3) utilizes excitation light (488 nm) from the expanded beam of an argon ion laser which is reflected by a dichroic mirror and focused at the rear focal plane of the TIRFM objective (Olympus 60×; numerical aperture = 1.45). Translation of the focusing lens allows introduction of the beam light either at the extreme edge of the objective lens for TIRF excitation, or more centrally for wide-field excitation. The emitted fluorescence is collected through the same objective and passed through a dichroic mirror (490 nm) and band-pass filter (510–600 nm) to a cooled, back-illuminated c.c.d. camera with on-chip electron multiplication (Cascade 128+; Roper Scientific). The camera provides full frame images (128 × 128 pixels; 1 pixel = 0.33 μm at the specimen) at a frame rate of 500 s^{-1}, with yet faster speeds possible by pixel-binning or selection of sub-frame regions. Accessory features include an autofocus device to

correct for focus drift during long recordings, and a photolysis light path for use with caged agonists such as carbamycholine and NMDA (Fig. 3).

5. Optical measurements of channel gating

Analogous to electrophysiological patch-clamp recording, TIRFM imaging provides kinetic information of ion channel gating. For example, Fig. 4A and B shows representative traces of SCCaFTs resulting from Ca^{2+} flux through muscle nicotinic receptors (αβγδ nAChR) activated by different agonists. SCCaFTs evoked by ACh (Fig. 4A) were relatively brief, and the distribution of SCCaFT durations was well fitted by an exponential with a time constant of 7.9 ms (Fig. 4C); a value that correspond to the open lifetime of the channel in similar experimental conditions [36,37]. Conversely, suberyldicholine, an agonist that evokes longer channel openings [37,38] generated SCCaFTs with a mean duration of 15.8 ms (Fig. 4B). Moreover, the concentration-dependence of channel opening may be derived by equilibrating different concentrations of agonist in the bathing solution.

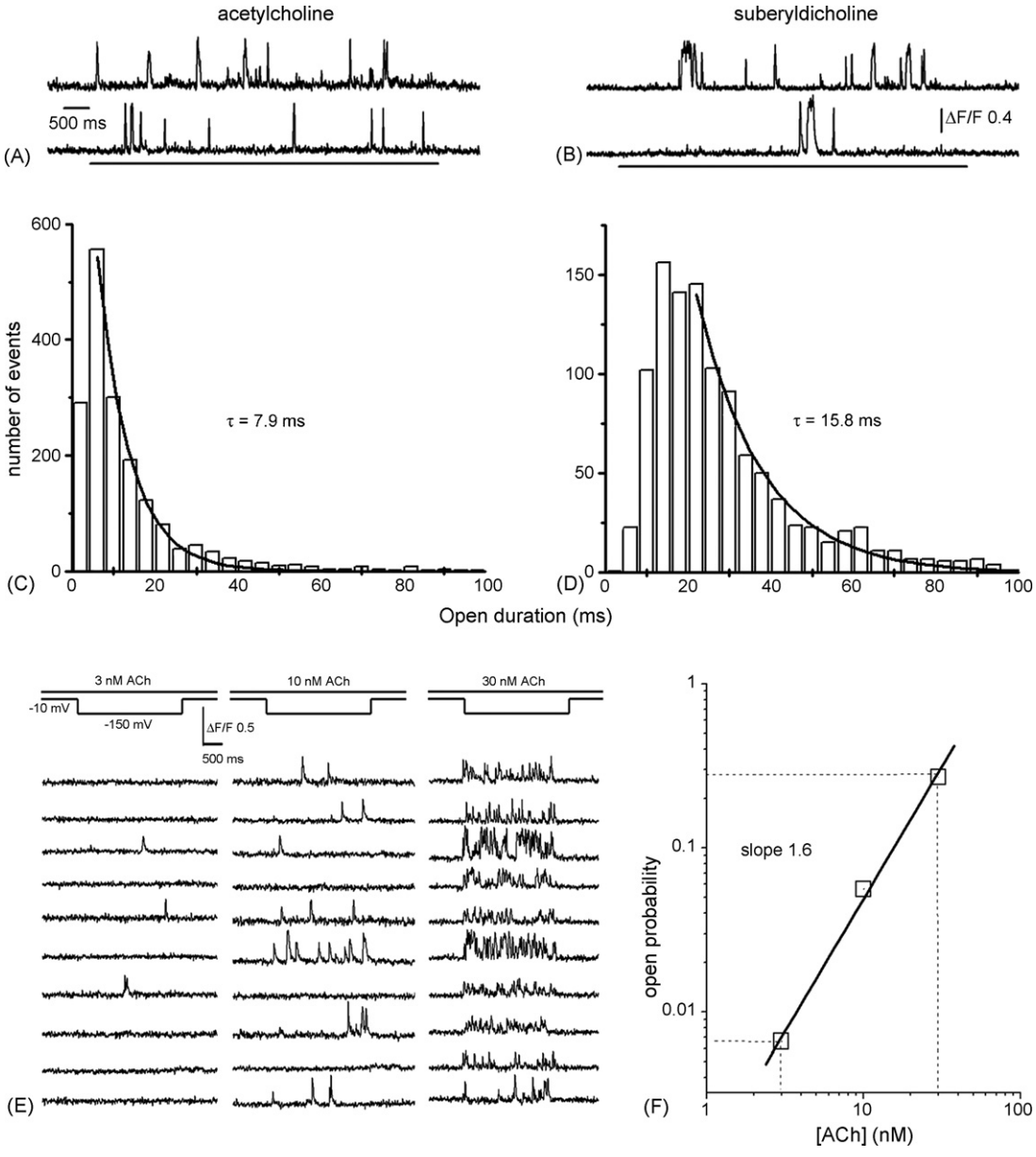

Fig. 4. Optical-patch clamp recording provides kinetic measurements of ion channel gating with temporal resolution of a few ms. (A) Traces show SCCaFTs evoked from two fetal muscle nicotinic AChR channels by 30 nM ACh. (B) SCCaFTs evoked from fetal muscle nicotinic AChR channels by 1 μM suberyldicholine. (C and D) Distributions of SCCaFT durations evoked, respectively, by ACh and suberyldicholine. Curves are single exponentials, with respective time constants of 7.9 and 15.8 ms. (E) Dose-dependence of SCCaFT activation. Representative traces show SCCaFTs evoked at the same 10 nAChR channel sites while [ACh] was successively changed from 3, 10 and 30 nM. (F) Relation between [ACh] in the bathing solution and mean channel open probability. Data are reproduced with permission from Ref. [21].

Fig. 4E shows traces illustrating the increase in SCCaFT frequency during application of increasing concentration of ACh. A plot of the open probability (mean proportion of the total time for which channel sites showed SCCaFTs) versus agonist concentration on double-logarithmic coordinates yielded a slope of about 1.6, consistent with the cooperativity derived from electrophysiological experiments [37].

6. Massively-parallel and spatially-resolved single-channel imaging

Optical imaging can thus resolve the gating of Ca^{2+}-permeable channels with a fidelity that now approaches that of patch-clamping. Moreover, 'optical patch-clamping' has major advantages of being massively parallel, allow-

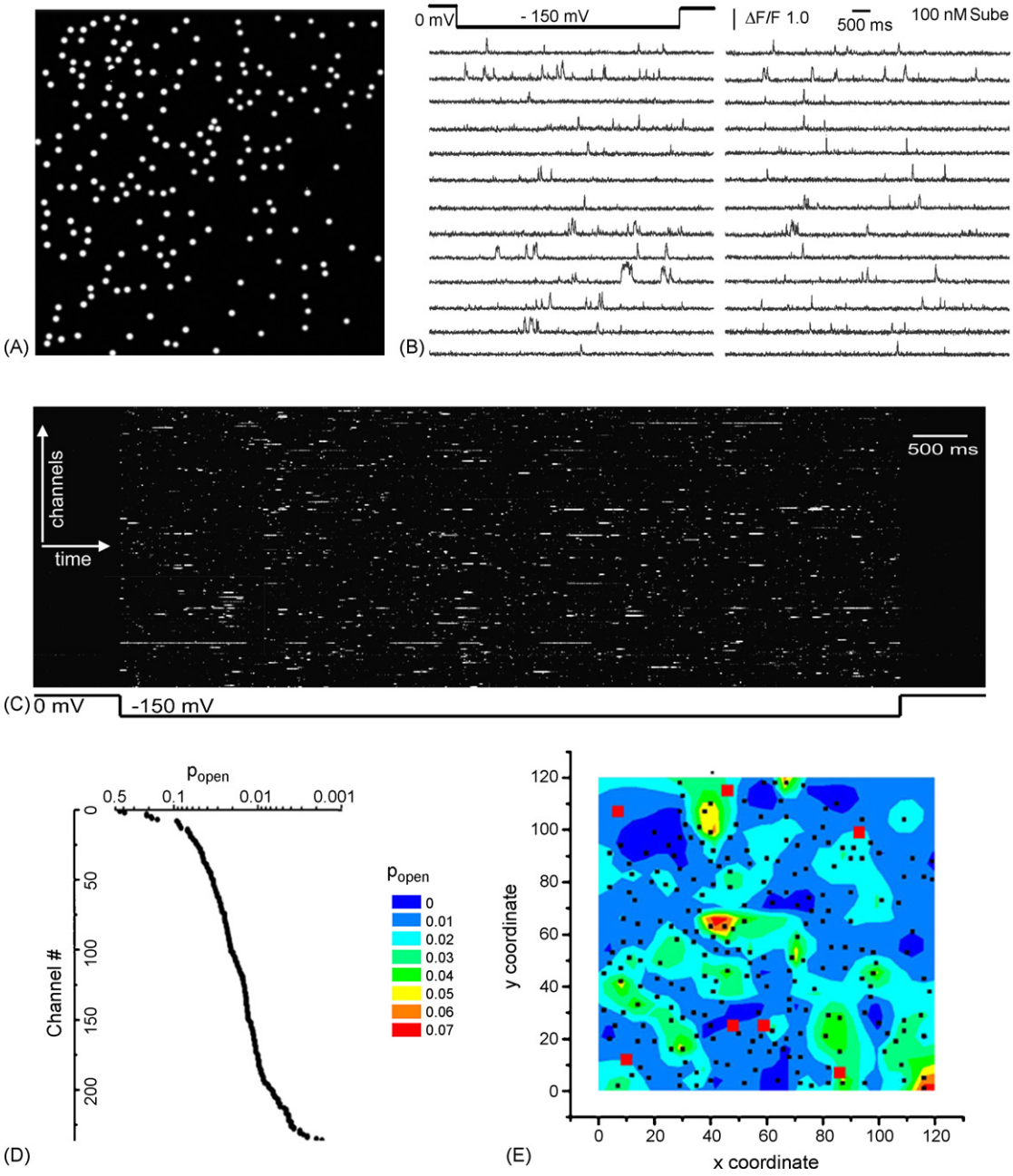

Fig. 5. Spatial and functional mapping of single channels. (A) Map showing the locations of 191 expressed nAChR channels (SCCaFT sites) within a 40 μm × 40 μm region of oocyte membrane. (B) Examples of selected single channel recording obtained from 28 of the channel sites marked in (A). (C) Channel–chip representation showing the activity of 236 channel imaged in a different experiment. The channel opening are depicted as white streaks, time runs from left to right, and the channels are stacked vertically in random order. The oocyte potential was stepped from 0 to −150 mV as indicated to increase the driving force for Ca^{2+} influx. (D) Variation in mean channel open probability (P_{open}) among the 236 channels. (E) Color contour plot showing the distribution of open probability (P_{open}) of all the 236 channels throughout a 40 μm × 40 μm imaging field. Contours depict mean P_{open} on 30 × 30 grid matrix, with different colors corresponding to P_{open} values as indicated by the scale. Modified, and reproduced with permission from Ref. [21]. (For interpretation of the references to color in this figure legend, the reader is referred to the web version of the article.)

ing simultaneous measurement from hundreds of Ca^{2+}-permeable channels, as well as providing spatial information of channel locations. This is illustrated in Fig. 5A, where the locations of 191 nAChR channels expressed in a 40 μm square of oocyte membrane were mapped by visually identifying all SCCaFT coordinates observed during an 8 s hyperpolarizing pulse to −150 mV in the presence of 100 nM suberyldicholine. Fortuitously, all channels that have so far been imaged appear to be rigidly anchored [20,21]. Multiple repeated SCCaFTs can thus be recorded for prolonged periods (minutes) from fixed regions of interest centered on channel sites, and channel locations can be inferred from the centroids of the fluorescence transients with a resolution appreciably better (<100 nm) than the diffraction-limit of the microscope [21].

The high throughput of TIRFM single-channel imaging presents considerable challenges in terms of data acquisition, analysis and display. One minute of recording at 500 frames s^{-1} generates a roughly 1 GB raw image file, which may contain data from several hundred channels. We thus developed a novel graphical representation, the "channel-chip" (Fig. 5C), wherein the activity of multiple channels is encapsulated in a single image to provide an immediate overview [21]. For example, it is evident from Fig. 5C that the gating kinetics differ widely from channel to channel, resulting in a broad spread of mean open probabilities (Fig. 5D). Finally, optical imaging enables not only positional mapping, but also functional mapping to reveal whether channel properties may be regulated according to their location [21]. Thus, far we have not found clear evidence for spatially-correlated variation in properties of channels expressed in the oocyte (Fig. 5E), but TIRFM imaging of L-type channels in smooth muscle has revealed specific sites of coordinated, high probability openings [23].

7. Perspective and future applicability of single-channel Ca^{2+} imaging

The technique of monitoring single-channel ion flux via optical imaging is likely to remain restricted to Ca^{2+}-permeable channels, primarily because the resting cytosolic Ca^{2+} levels are maintained much lower than that of other ions so that influx results in enormous local increases in concentration that are readily detectable by fluorescence indicator dyes. Nevertheless, numerous types of ion channels show appreciable permeability to Ca^{2+} (summarized in Table 1), so imaging of SCCaFTs has widespread potential applicability. The various families of voltage-gated Ca^{2+} channels are the most obvious mechanisms for regulating plasma membrane Ca^{2+} flux, but growing evidence emphasizes also the importance of numerous ligand-gated channels [39–45], among which attention has focused on nAChRs and ionotropic glutamate receptors (GluR) because of their involvement in synaptic transmission.

In terms of applicability for optical single-channel imaging an obvious prerequisite is that sufficient Ca^{2+} passes through the channel to provide a detectable fluorescence signal. In practice, a surprisingly high sensitivity can be attained. A channel with a unitary Ca^{2+} current of 0.1 pA opening for 10 ms corresponds to a flux of about 3000 Ca^{2+} ions, generating a few hundred Ca^{2+}-bound indicator molecules within the sub-femtolitre volume sampled by the point-spread function of a confocal or TIRF microscope [30]. Since dyes molecules such as fluo-4 can readily be excited to emit >10^4 photons s^{-1} this provides a strong optical signal even after taking into account losses in collection efficiency in the microscope and quantum efficiency of the detector. Thus, we have obtained records with good temporal resolution (2 ms) and signal-to-noise ratio from fetal nAChR that have a Ca^{2+} conductance of less than 1 pS (Table 1) by hyperpolarizing the membrane to generate predicted Ca^{2+} currents of a few hundred fA

Table 1
Plasma membrane ion channels with Ca permeability

		P_f (%)	γ (pS)	$\gamma_{(Ca)}$ (pS)		P_f (%)	γ (pS)	$\gamma_{(Ca)}$ (pS)
nAChRs – muscle – adult (α, β, δ, ε)		4	~ 60 [40,42,46]	2.4	Caffeine channels	20	80 [40,49]	16
nAChRs – muscle – fetal (α, β, γ, δ)		2	~ 40 [40,42,46]	0.8	CNG-channels (CNCα1-α4;β1)	~0.6	~28 [50]	17
nAChRs – neuronal – (α2–6, β2–4)		2-5	~32-45 [43,46]	0.6-2.3	VGCC – L-type	[51]		13
nAChRs – neuronal – (α7-α9)		20	~19-23 [43,46]	3.8-4.6	VGCC – T-type	[52]		7
NMDA → (NR1, NR2A - NR2D)		8-12	~18-50 [47,48]	1.4-6	VGCC – N-type	[53]		13
AMPA → (GluR-A, -C, -D)		4	~10-20	0.4-0.8	VGCC – P/Q type	[54]		~11
AMPA → (GluR-B)		0.1			TRP – TRPC (Classic)	40-50	~ 110-135 [55]	~ 40-65
Kainate → (GluR5-7)		0.2-0.7	~1.5-6 [47,48]	> 0.04	TRP – TRPM (Melastatin)	40-70	~ 40-130	~ 16-90
ATP channels → (P2x1 to P2X7)		2-10	~9-20 [40,49]	0.2-2	TRP – TRPV (Vanilloid)	1-100	~35-172 [55]	~4-80
					SAC (stretch-activated channels)	18	13 [56]	2.3

P_f is the fractional Ca^{2+} permeability, measured by electrophysiological or fluorescence techniques, in the presence of 10–60 mM extracellular Ca^{2+}: γ is the total cation conductance: $\gamma_{(Ca)}$ is calculated as $\gamma \cdot P_f$. Single-channel imaging has been achieved with those channels marked by shading.

[21]. Indeed, optical imaging may actually be superior to patch-clamp recording for monitoring Ca^{2+} currents under physiological conditions. For example, patch-clamp experiments recording from voltage-gated Ca^{2+} channels usually employ high concentrations of Ba^{2+} as the charge carrier to increase the single channel current, whereas SCCaFTs are readily imaged using only modestly elevated (ca. 6 mM) extracellular [Ca^{2+}], and remain detectable even at physiological [Ca^{2+}] [13,22,23,34].

Table 1 summarizes many of the channel types that are likely candidates for 'optical patch-clamp' recording. Estimates of the fractional Ca^{2+} conductance (conductance to Ca^{2+} ions as a percentage of the total conductance to all cations under physiological conditions) reveal a wide range between different channel types, with values ranging from as low as 0.2% for kainate receptors to almost 100% for voltage-gated Ca^{2+} channels. However, it is not simply the fractional Ca^{2+} permeability that is important for single-channel Ca^{2+} imaging, but rather the absolute single-channel Ca^{2+} flux. For example, the Ca^{2+} conductance of the fetal type nAChR is only about 30% that of the adult type, owing both to a lower fractional Ca^{2+} permeability and to a smaller overall cation conductance. The fact that good records of SCCaFTs can be obtained from fetal nAChR – which have among the lowest Ca^{2+} conductance of all channels listed in Table 1 – thus bodes well for the general utility of this technique.

In conclusion, TIRFM imaging enables imaging of Ca^{2+} microdomains around single plasma-membrane channels with unprecedented temporal and spatial resolution. We anticipate that this technique will evolve as a powerful adjunct to electrophysiological techniques for studying channel gating and permeation properties, with the particular advantage of being massively parallel. Moreover, it affords spatial information of channel location, and provides a direct, if slightly blurred, visualization of the fate of Ca^{2+} ions that enter the cytosol.

Acknowledgements

We thank Drs. Jianwei Shuai and Heather Rose for many helpful discussions. Work in the authors' laboratory is supported by grants GM 48071 and GM 65830 from the National Institutes of Health.

References

[1] M. Berridge, P. Lipp, M. Bootman, Calcium signalling, Curr. Biol. 9 (1999) R157–R159.
[2] M.J. Berridge, M.D. Bootman, P. Lipp, Calcium–a life and death signal, Nature 395 (1998) 645–648.
[3] M.J. Berridge, P. Lipp, M.D. Bootman, The versatility and universality of calcium signalling, Nat. Rev. Mol. Cell Biol. 1 (2000) 11–21.
[4] M.J. Berridge, P. Lipp, M.D. Bootman, Signal transduction. The calcium entry pas de deux, Science 287 (2000) 1604–1605.
[5] M.D. Bootman, M.J. Berridge, P. Lipp, Cooking with calcium: the recipes for composing global signals from elementary events, Cell 91 (1997) 367–373.
[6] M.D. Bootman, T.J. Collins, C.M. Peppiatt, L.S. Prothero, L. MacKenzie, P. De Smet, M. Travers, S.C. Tovey, J.T. Seo, M.J. Berridge, F. Ciccolini, P. Lipp, Calcium signalling—an overview, Semin. Cell Dev. Biol. 12 (2001) 3–10.
[7] E. Neher, Usefulness and limitations of linear approximations to the understanding of Ca^{++} signals, Cell Calcium 24 (1998) 345–357.
[8] R. Yuste, L.C. Katz, Control of postsynaptic Ca^{2+} influx in developing neocortex by excitatory and inhibitory neurotransmitters, Neuron 6 (1991) 333–344.
[9] R. Yuste, A. Majewska, K. Holthoff, From form to function: calcium compartmentalization in dendritic spines, Nat. Neurosci. 3 (2000) 653–659.
[10] G. Grynkiewicz, M. Poenie, R.Y. Tsien, A new generation of Ca^{2+} indicators with greatly improved fluorescence properties, J. Biol. Chem. 260 (1985) 3440–3450.
[11] M.J. Berridge, Elementary and global aspects of calcium signalling, J. Exp. Biol. 200 (1997) 315–319.
[12] I. Parker, Y. Yao, Regenerative release of calcium from functionally discrete subcellular stores by inositol trisphosphate, Proc. Biol. Sci. 246 (1991) 269–274.
[13] H. Cheng, W.J. Lederer, M.B. Cannell, Calcium sparks: elementary events underlying excitation-contraction coupling in heart muscle, Science 262 (1993) 740–744.
[14] P. Lipp, E. Niggli, Fundamental calcium release events revealed by two-photon excitation photolysis of caged calcium in Guinea-pig cardiac myocytes, J. Physiol. 508 (Pt 3) (1998) 801–809.
[15] I. Parker, Y. Yao, Ca^{2+} transients associated with openings of inositol trisphosphate-gated channels in *Xenopus* oocytes, J. Physiol. 491 (Pt 3) (1996) 663–668.
[16] S.Q. Wang, L.S. Song, E.G. Lakatta, H. Cheng, Ca^{2+} signalling between single L-type Ca^{2+} channels and ryanodine receptors in heart cells, Nature 410 (2001) 592–596.
[17] H. Zou, L.M. Lifshitz, R.A. Tuft, K.E. Fogarty, J.J. Singer, Visualization of Ca^{2+} entry through single stretch-activated cation channels, Proc. Natl. Acad. Sci. U.S.A. 99 (2002) 6404–6409.
[18] H. Zou, L.M. Lifshitz, R.A. Tuft, K.E. Fogarty, J.J. Singer, Imaging Ca^{2+} entering the cytoplasm through a single opening of a plasma membrane cation channel, J. Gen. Physiol. 114 (1999) 575–588.
[19] A. Demuro, I. Parker, Optical single-channel recording: imaging Ca^{2+} flux through individual N-type voltage-gated channels expressed in Xenopus oocytes, Cell Calcium 34 (2003) 499–509.
[20] A. Demuro, I. Parker, Imaging single-channel calcium microdomains by total internal reflection microscopy, Biol. Res. 37 (2004) 675–679.
[21] A. Demuro, I. Parker, Optical patch-clamping": single-channel recording by imaging Ca^{2+} flux through individual muscle acetylcholine receptor channels, J. Gen. Physiol. 126 (2005) 179–192.
[22] M.F. Navedo, G.C. Amberg, M. Nieves, J.D. Molkentin, L.F. Santana, Mechanisms underlying heterogeneous Ca^{2+} sparklet activity in arterial smooth muscle, J. Gen. Physiol. (2006).
[23] M.F. Navedo, G.C. Amberg, V.S. Votaw, L.F. Santana, Constitutively active L-type Ca^{2+} channels, Proc. Natl. Acad. Sci. U.S.A. 102 (2005) 11112–11117.
[24] A. Demuro, I. Parker, Optical single-channel recording: imaging Ca^{2+} flux through individual ion channels with high temporal and spatial resolution, J. Biomed. Opt. 10 (2005) 11002.
[25] I. Parker, Plasmalemmal Ca^{2+} signaling in arterial smooth muscle: it's elementary!, J. Gen. Physiol. 127 (2006) 605–609.
[26] S.Q. Wang, C. Wei, G. Zhao, D.X. Brochet, J. Shen, L.S. Song, W. Wang, D. Yang, H. Cheng, Imaging microdomain Ca^{2+} in muscle cells, Circ. Res. 94 (2004) 1011–1022.
[27] H. Zou, L.M. Lifshitz, R.A. Tuft, K.E. Fogarty, J.J. Singer, Imaging calcium entering the cytosol through a single opening of plasma membrane ion channels: SCCaFTs—fundamental calcium events, Cell Calcium 35 (2004) 523–533.

[28] P. Lipp, E. Niggli, Submicroscopic calcium signals as fundamental events of excitation—contraction coupling in guinea-pig cardiac myocytes, J. Physiol. 492 (Pt 1) (1996) 31–38.
[29] E. Neher, Vesicle pools and Ca^{2+} microdomains: new tools for understanding their roles in neurotransmitter release, Neuron 20 (1998) 389–399.
[30] J. Shuai, I. Parker, Optical single-channel recording by imaging Ca^{2+} flux through individual ion channels: theoretical considerations and limits to resolution, Cell Calcium 37 (2005) 283–299.
[31] A.C. Ventura, L. Bruno, A. Demuro, I. Parker, S.P. Dawson, A model-independent algorithm to derive Ca^{2+} fluxes underlying local cytosolic Ca^{2+} transients, Biophys. J. 88 (2005) 2403–2421.
[32] X.P. Sun, N. Callamaras, J.S. Marchant, I. Parker, A continuum of InsP3-mediated elementary Ca^{2+} signalling events in *Xenopus* oocytes, J. Physiol. 509 (Pt 1) (1998) 67–80.
[33] H. Zou, L.M. Lifshitz, R.A. Tuft, K.E. Fogarty, J.J. Singer, Using total fluorescence increase (signal mass) to determine the Ca^{2+} current underlying localized Ca^{2+} events, J. Gen. Physiol. 124 (2004) 259–272.
[34] A. Demuro, I. Parker, Imaging the activity and localization of single voltage-gated Ca^{2+} channels by total internal reflection fluorescence microscopy, Biophys. J. 86 (2004) 3250–3259.
[35] D. Axelrod, Total internal reflection fluorescence microscopy in cell biology, Methods Enzymol. 361 (2003) 1–33.
[36] C.R. Anderson, C.F. Stevens, Voltage clamp analysis of acetylcholine produced end-plate current fluctuations at frog neuromuscular junction, J. Physiol. 235 (1973) 655–691.
[37] B. Hille, Ion Channels of Excitable Membranes, Sinauer Associates, Sunderland, Mass., 2001, pp. 814.
[38] D. Colquhoun, B. Sakmann, Fast events in single-channel currents activated by acetylcholine and its analogues at the frog muscle end-plate, J. Physiol. 369 (1985) 501–557.
[39] N. Burnashev, Calcium permeability of glutamate-gated channels in the central nervous system, Curr. Opin. Neurobiol. 6 (1996) 311–317.
[40] N. Burnashev, Calcium permeability of ligand-gated channels, Cell Calcium 24 (1998) 325–332.
[41] N. Burnashev, H. Monyer, R. Schoepfer, P. Seeburg, Calcium permeability of recombinant NMDA receptor channels, Soc. Neurosci. Abstracts 18 (1992) 395.
[42] S. Fucile, Ca^{2+} permeability of nicotinic acetylcholine receptors, Cell Calcium 35 (2004) 1–8.
[43] S. Fucile, M. Renzi, P. Lax, F. Eusebi, Fractional Ca^{2+} current through human neuronal alpha7 nicotinic acetylcholine receptors, Cell Calcium 34 (2003) 205–209.
[44] P. Lax, S. Fucile, F. Eusebi, Ca^{2+} permeability of human heteromeric nAChRs expressed by transfection in human cells, Cell Calcium 32 (2002) 53–58.
[45] S.J. Robertson, N. Burnashev, F.A. Edwards, Ca^{2+} permeability and kinetics of glutamate receptors in rat medial habenula neurones: implications for purinergic transmission in this nucleus, J. Physiol. 518 (Pt 2) (1999) 539–549.